Cyclotron Maser Oscillator Experiments in a Periodically Loaded Waveguide

Eli Jerby, Avi Shahadi, Vladimir Grinberg, Vladimir Dikhtiar, Marat Sheinin, Eran Agmon, Harel Golombek, Vitaly Trebich, Moshe Bensal, and G. Bekefi

***Abstract*—The periodic-waveguide cyclotron maser is a device in which orbiting, nonrelativistic electrons interact with traveling waves in a metallic, periodically loaded waveguide. In this paper, we describe a table-top oscillator experiment that operates in the microwave regime (9.4 GHz) with a low-energy (8 keV), low-current (0.2 A) electron beam pulse (1 ms pulse width). The frequency modulation (chirping) observed is used in the determination of cyclotron resonance condition for this interaction. The results show that the cyclotron interaction occurs with a backward-propagating wave in the periodically loaded waveguide. Microwave power of ≥ 0.3 kW and efficiency of $\geq 20\%$ are measured by an external loading of the oscillator.**

I. Introduction

THE periodic-waveguide cyclotron maser is a device in which orbiting, nonrelativistic electrons undergo a cyclotron interaction with traveling waves in a periodic waveguide. The device is shown in Fig. 1.

Our first periodic-waveguide cyclotron experiment has been conducted at MIT in an amplifier configuration [1], [2]. In that experiment, a low-energy electron beam (8 keV, 1 A) in an axial magnetic field of 3 kG interacted with an 8.2-GHz traveling wave. The system consisted of an array of metal posts in a standard rectangular WR90 waveguide. Cyclotron resonance conditions were studied under various experimental conditions. Electronic gain of ~10 dB was measured at the Doppler-shifted electron cyclotron resonance. Following the amplifier experiment at MIT, we then developed the oscillator experiment at Tel Aviv University [3], [4] as described in this paper.

The *slow-wave* properties of the periodic waveguides in our maser are similar to the dielectric-loaded slow-wave cyclotron (SWC) masers of earlier work [5]–[13]. Such schemes have been investigated in various dielectric waveguides in order to increase the interaction bandwidth and to reduce the necessary electron beam energy as compared with respect to the more conventional *fast-wave* cyclotron masers [14]–[18].

The dominant mechanism of the SWC interaction differs from that of the fast wave cyclotron masers. In the SWC, the dominant electron bunching stems from the $\boldsymbol{V}_\perp \times \boldsymbol{B}_\perp$ axial force component (i.e., the Weibel instability), whereas the dominant effect in the fast-wave cyclotron devices is the relativistic azimuthal bunching that results from the transverse electron energy variation due to the nonzero $\boldsymbol{V}_\perp \cdot \boldsymbol{E}_\perp$ term (where $\boldsymbol{V}_\perp$ is the electron transverse velocity component and $\boldsymbol{E}_\perp$, $\boldsymbol{B}_\perp$ are the transverse electric and magnetic components of the electromagnetic wave). Although the interaction with slow waves increases the bandwidth, a much-desired property, it unfortunately makes the interaction more sensitive to the electron beam spread (i.e., temperature).

A recent theoretical study of the periodic-waveguide cyclotron interaction [19] discusses the differences between this mechanism and that of the dielectric SWC masers. From the technical point of view, the use of a metallic periodic waveguide, rather than a dielectric-loaded waveguide, alleviates some technical difficulties (surface charging) that result from the presence of a dielectric insulator in the vicinity of a high-power electron beam. Thus, the periodic-waveguide cyclotron maser is expected to be a more practical low-voltage cyclotron-type device.

In the next sections we present the table-top experimental setup and describe the experimental results. The theory of the periodic-waveguide cyclotron maser is summarized in the next section.

II. Theory

The cyclotron device shown in Fig. 1 consists of a periodically-loaded waveguide along which a low-energy electron beam is orbiting in an externally applied axial magnetic field. The orbiting motion of the electrons couples them to a spatial harmonic of the electro-magnetic wave in the periodic waveguide. The tuning relation of a cyclotron interaction with the nth spatial harmonic is given by

$$\omega = \omega_c + V_{0z}\beta_n(\omega) \tag{1}$$

where ω is the em wave angular frequency. The angular cyclotron frequency is

$$\omega_c = \frac{e}{\gamma m}B_0, \tag{2}$$

where e, m, γ, and V_{0z} are the electron charge, mass, relativistic factor, and axial velocity, respectively, and B_0 is the axial magnetic field. The wavenumber of the nth-order spatial

Manuscript received May 17, 1994; revised November 27, 1994. This research is supported in part by the Israeli Ministry of Energy, The Belfer Foundation for Energy Research, and the Israeli Ministry of Absorption.

E. Jerby, A. Shahadi, V. Grinberg, V. Dikhtiar, M. Sheinin, E. Agmon, H. Golombek, V. Trebich, and M. Bensal are with the Faculty of Engineering, Tel Aviv University, Ramat Aviv 69978, Israel.

G. Bekefi is with the Department of Physics and Research Laboratory of Electronics, Massachusetts Institute of Technology, Cambridge, MA 02139 USA.

IEEE Log Number 9409845.

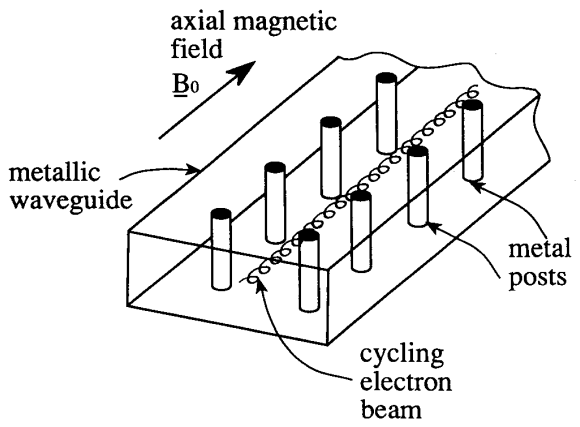

Fig. 1. Schematic of a periodic waveguide Cyclotron device.

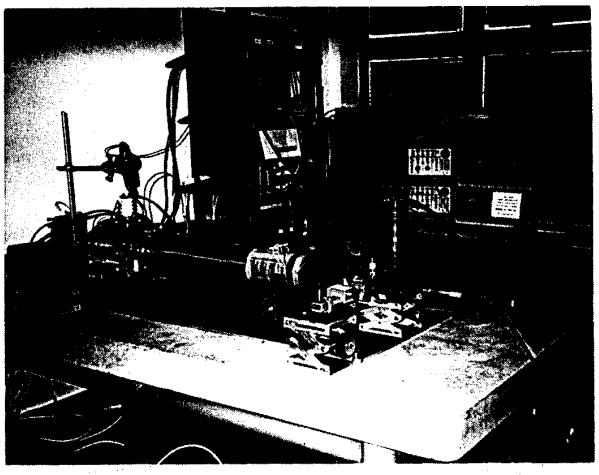

Fig. 2. A general view of the experimental setup.

harmonic, $\beta_n(\omega)$, is determined by the periodic waveguide dispersion relation.

A theoretical model of the traveling wave cyclotron interaction [19] shows that in the linear regime the convective cyclotron interaction with the nth spatial harmonic is described by a Pierce-type dispersion equation, where the amplitude growth rate $A(z)$ is given in the Laplace $\hat{s}$ space by

$$\tilde{A}(\hat{s}) = \frac{(\hat{s}-\hat{\theta}_n)^2}{\hat{s}(\hat{s}-\hat{\theta}_n)^2 - \frac{1}{2}\kappa_n(\hat{s})F_{f_n}C_n(\hat{s})\hat{\theta}_p^2}A_0. \quad (3)$$

Here $\kappa_n(\hat{s})$ is the complex coupling coefficient of the interaction given by

$$\kappa_n(\hat{s}) = \overbrace{\overline{\beta}_{ez}(\hat{s}-\hat{\theta}_n)(\hat{Z}_n}^{e1} - \overbrace{\overline{\beta}_{ez}}^{e2}) + \frac{1}{2}\overline{\beta}_{e\perp}^2(\overbrace{\hat{k}\hat{Z}_n}^{e3} - \overbrace{\hat{s}-\hat{\beta}_n}^{e4}). \quad (4)$$

The dimensionless operating parameters in (3) and (4) are defined as follows. The tuning parameter for the nth harmonic is $\hat{\theta}_n = (\omega - \omega_c)\tau_0 - \hat{\beta}_n$, where $\tau_0 = L/V_{0z}$ is the electron time of flight along the interaction length L. The normalized space-charge parameter is $\hat{\theta}_p = \omega_p\tau_0$ where ω_p is the relativistic electron plasma frequency, and the dimensionless wavenumbers are defined as $\hat{s} = jsL$, $\hat{k} = kL$, and $\hat{\beta}_n = \beta_n L$. The parameters of the nth spatial harmonic in (4) are the filling factor and the coupling factor, F_{f_n} and $C_n(\hat{s})$, respectively, and the normalized harmonic impedance $\hat{Z}_n$ [19]. The electron average normalized axial and perpendicular velocity components are $\overline{\beta}_{ez}$ and $\overline{\beta}_{e\perp}$, respectively.

The gain-dispersion equation (3) resembles the Pierce equation, which is valid in general for a wide range of traveling wave devices and free-electron lasers. The coupling term (4), however, is more complicated. It incorporates four different effects denoted by the $e1$ to $e4$ shown with overbraces in (4). Each effect dominates in a different parameter regime. For zero initial transverse electron velocity component, $\overline{\beta}_{0\perp} = 0$, only the $e1$ and $e2$ terms exist in (4). The term denoted by $e2$ is dominant when $\hat{Z}_n < \overline{\beta}_{ez}$, i.e., when the normalized harmonic impedance is smaller than the normalized electron velocity. In this regime, as analyzed in [19], the device acts as an amplifier. The $e2$ effect is believed to be the dominant mechanism in the amplifier experiment at MIT [2] in which no means were used to spin up the electrons at the entrance to the interaction region.

The term denoted by $e1$ in (4) is dominant in a uniform waveguide (no metal posts) in which $\hat{Z}_0 > \overline{\beta}_{ez}$. This effect involves a transverse acceleration of the e-beam by the electromagnetic wave. When it dominates, the wave is attenuated. However, for $\overline{\beta}_{0\perp}$ sufficiently large gain occurs. Here the term denoted by $e3$ represents the azimuthal bunching effect, which characterizes the fast cyclotron resonance maser (CRM) devices in uniform, unloaded, waveguides. The term denoted by $e4$ represents an axial bunching effect known as the Weibel interaction. The latter is the dominant effect in the dielectric-loaded SWC interaction [5]–[13]. The terms $e3$ and $e4$, which correspond to the azimuthal and the axial bunching effects, respectively, compete and oppose one another.

III. Experimental Setup

A general view of the table-top experimental setup is shown in Fig. 2. The apparatus is based on the traveling-wave free-electron maser (TWFEM) experiment [20] at Tel Aviv University. The oscillator tube consists of a Pierce-type electron gun, a periodic waveguide, a solenoid, and a kicker electromagnet. The latter imparts transverse velocity ($V_{0\perp}$) to the electrons. A low-energy electron beam (<10 keV) is injected on-axis into the periodic waveguide and interacts with the traveling waves. The uniform solenoidal magnetic field maintains the electron cyclotron motion along its axis. The electron beam is dumped at the exit of the interaction region onto a collector, which is also used to measure the electron current.

A block diagram of the experimental setup is shown in Fig. 3. Three synchronized pulsers generate the solenoid, the e-gun, and the kicker pulses. The e-gun high-voltage pulser (10 kV, 0.25 A, 1 ms) and the high-current kicker pulser

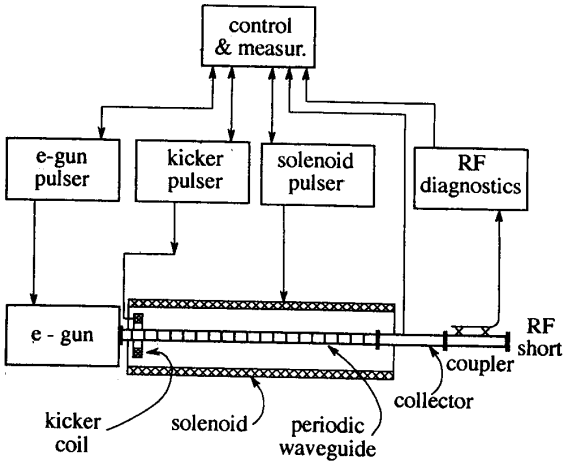

Fig. 3. A block diagram of the oscillator experimental setup.

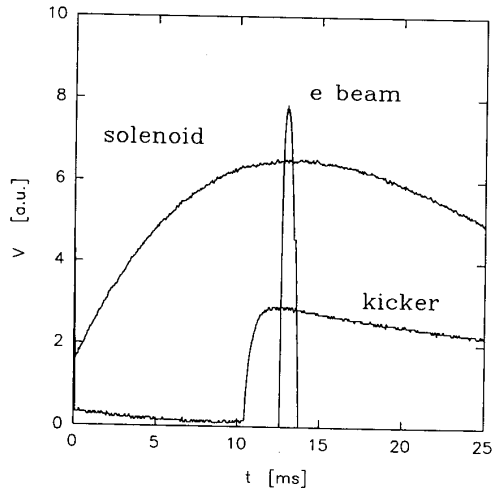

Fig. 4. A timing diagram of the solenoid, the kicker, and the e-gun pulses.

are triggered at the peak of the solenoid pulse as shown in the timing diagram of Fig. 4. The main components of the periodic-waveguide cyclotron oscillator experiment are described in more detail in the following sections.

A. Periodic Waveguide

In the present oscillator experiment, we use an inductive periodic waveguide similar to the MIT amplifier experiment. This waveguide, shown in Fig. 1, consists of an array of metal posts inserted into a standard WR90 rectangular waveguide. The dimensions of the periodic waveguide are given in Table I, with a glossary of the notation used in this paper. The waveguide length and post diameter differ somewhat from that of the MIT waveguide. The larger post diameter (1.9 mm comparing to 1.0 mm at MIT) results in a higher waveguide cutoff frequency in the oscillator experiment.

TABLE I
EXPERIMENTAL PARAMETERS

electron beam			
energy	U_0	8	[keV]
current	I_{eb}	0.2	[A]
pulsewidth		1	[ms]
Magnetic field			
solenoid	B_0	4	[kG]
kicker		7	[kA turns]
Periodic waveguide			
rectangular tube	$a \times b$	0.9×0.4	[inch^2]
metal post array:			
periodicity	p	20	[mm]
post diameter	$2r_p$	1.9	[mm]
post distance	d	6.4	[mm]
length	L	54	[cm]
Electromagnetic wave			
frequency	f	9.4	[GHz]
output power		> 0.3	[kW]

The dispersion relation $\omega(\beta_0)$ of a lossless periodic waveguide, which consists of a periodic array of lumped inductive elements is given by [21]:

$$\cos(\beta_0 p) = \cos(k_{10} p) + \frac{1}{2}\overline{B}\sin(k_{10} p) \tag{5}$$

where $k_{10} = \sqrt{(\omega/c)^2 - (\pi/a)^2}$ is the wavenumber of the fundamental TE_{10} mode, and p is the waveguide period. (5) is valid when all higher modes are evanescent and their decay lengths are much shorter than the waveguide period.

The normalized inductive susceptance of a single pair of posts in a waveguide is given by [22]

$$\overline{B} \cong \frac{\lambda_g}{a}\left\{\frac{(1+\sqrt{2})}{4}\frac{\pi r_p}{a} + \frac{\ln[(2a/\pi r_p)\tan(\pi d/a)]}{4\sin^2(\pi d/a)} + \frac{2}{3}\left[\frac{a}{3\lambda}\frac{\sin(3\pi d/a)}{\sin(\pi d/a)}\right]^2 - 1\right\}^{-1} \tag{6}$$

where r_p is the post radius ($r_p \ll a$), and $\lambda_g = 2\pi/k_{10}$ and $\lambda = 2\pi c/\omega$ are the waveguide and free-space wavelengths, respectively.

Cold measurements (in the absence of the electron beam) of the periodic waveguide (28 pairs of posts, 60 cm length, 2 mm post diameter) were done on an HP 8757A network analyzer shown in Fig. 5(a). The transmission and reflection measurements (i.e., the waveguide $|S_{21}|^2$ and $|S_{11}|^2$ scattering parameters, or the insertion and reflection losses, respectively) are shown in Fig. 5(b) and (c). The first passband of the periodic waveguide is in the frequency range of 9.23 GHz to 10.14 GHz. The transmission curve shows 26 maxima at different frequencies. Each maximum corresponds to a

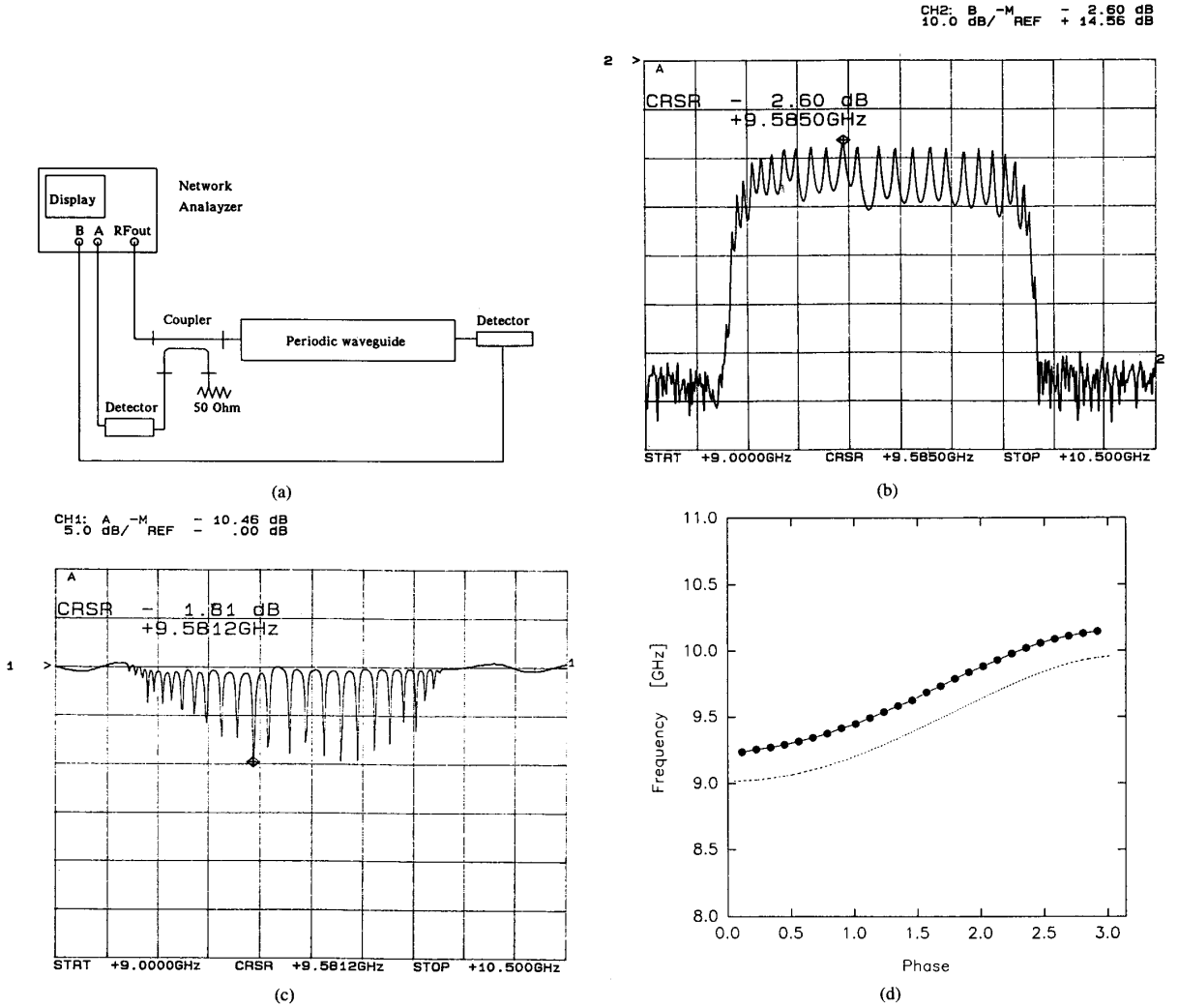

Fig. 5. Periodic waveguide measurements. (a) The scalar network analyzer measurement setup. (b) The measured transmission curve. (c) The measured reflection curve. (d) The dispersion curves obtained from measurements (dots) and theory (solid line).

minimum in the reflection curve, as expected. These extremum points represent the resonance frequencies of the finite periodic waveguide and result from the reflections at both ends of the system. The transmission maxima satisfy the resonance condition

$$\phi_s = \beta_{0s} L = s\pi \qquad \forall s = 1, 2 \cdots 26. \tag{7}$$

where $L = 28p$. Hence, an integer number of half-periods of wavelength $2\pi/\beta_0$ are spaced over the entire periodic waveguide length L for the forward and backward waves. This measurement provides a simple way to construct the dispersion diagram $\omega(\beta_0)$ of the periodic waveguide as proposed in [23]. The dots in Fig. 5(d) show the sth transmission frequency maxima versus the corresponding $\beta_{0s} = s\pi/L$ wavenumbers (for $s = 1$ to 26) as obtained from the transmission measurement in Fig. 5(b). This experimental result is compared with the theoretical dispersion relation (dashed line) found from (5). The 2% deviation between the calculated and measured dispersion curves in Fig. 5(d) stems from the neglect of the resistive losses, the post capacitance [24], and the evanescent modes in (5).

The periodic array used in the cyclotron oscillator experiment is 54 cm long. It is tapered at the input end to improve impedance matching to the waveguide (the far end from the electron entrance is shorted). Due to vacuum considerations, the periodic waveguide used in the cyclotron experiment consists of a "nail-bed" structure inserted into the rectangular waveguide. The microwave performance of this arrangement might be somewhat inferior to welded posts due to imperfect contacts between post tips and the waveguide wall. The cold measurements shown in Fig. 5(b) and (c) are made on a welded post waveguide. However, this "welded" waveguide was later tested in the maser device after the completion of this paper and produced results similar to those of the insert nail-bed arrangement.

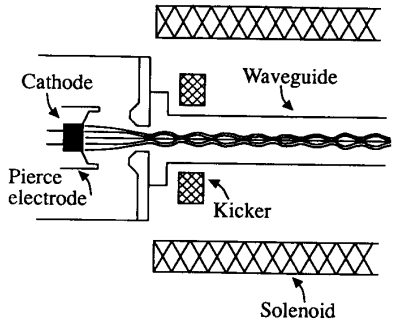

Fig. 6. The electron-optics apparatus.

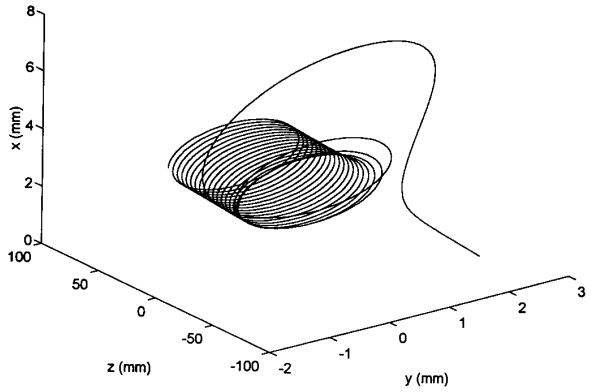

Fig. 7. The effect of a small kicker coil located in $z = 0$ on an electron with zero initial transverse velocity. Cyclotron motion is induced by the kicker acting on the electron.

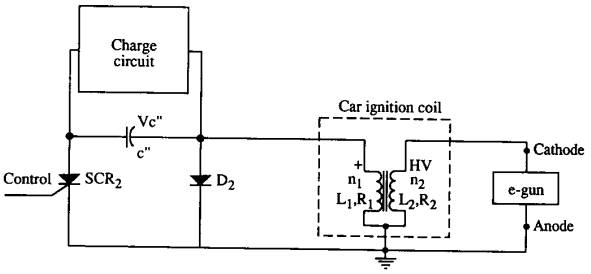

Fig. 8. Schematic of the electron gun pulser.

B. Electron Beam

The low-energy electron beam (< 10 keV) is generated by a Pierce-type electron gun. The electron gun developed for this experiment [25] consists of a dispenser thermionic cathode (Spectra-Mat, STD200) and electrostatic focusing Pierce electrode. The electron optics shown schematically in Fig. 6 consists of a kicker coil that induces the electron transverse velocity component, and a 4-kG solenoidal field. The waveguide is terminated by a collector section connected to ground by a 10-Ω resistor. The voltage drop on this resistor during the pulse yields the electron current.

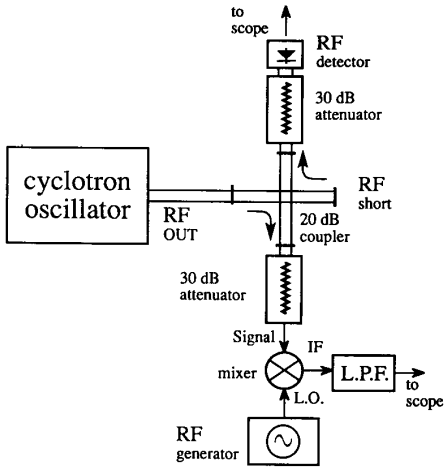

Fig. 9. The microwave diagnostic setup. It includes power measurements and frequency heterodyne detection.

The kicker coil spins up the electron beam. Its effect can be represented by two uncoupled equations [26], namely

$$\alpha' - \sqrt{\frac{e}{2m\Phi(z)}}\left[\frac{B(z)}{2} + \frac{C_0}{r^2}\right] = 0 \tag{8a}$$

$$\Phi(z)r'' + \frac{1}{2}\Phi' r' + \left[\frac{1}{4}(\Phi'' + \rho_0/\epsilon_0) + \frac{e}{8m}B(z)^2\right]r - \frac{e}{2m}C_0^2 r^{-3} = 0 \tag{8b}$$

where r and α are the radius and phase of the electron trajectory in cylindrical coordinates, $\Phi(z)$ is the electric potential on-axis, $B(z)$ is the axial magnetic field component on-axis, ρ_0 is the electron charge density, and r_0, α_0, and B_0 are the initial values of r, α and B respectively. The prime in (8a, b) denotes a derivative over z (i.e., $\alpha' = d\alpha/dz$). The parameter C_0 is given by $C_0 = mr_0^2\dot{\alpha}_0/e - B_0 r_0^2/2$. The kicker field on-axis is approximated [26] by

$$B(z) = \frac{\mu_0 N I_k}{2(r_2 - r_1)l}\left\{\left(z + \frac{l}{2}\right)\ln\frac{r_2 + \sqrt{r_2^2 + \left(z + \frac{l}{2}\right)^2}}{r_1 + \sqrt{r_1^2 + \left(z + \frac{l}{2}\right)^2}} - \left(z - \frac{l}{2}\right)\ln\frac{r_2 + \sqrt{r_2^2 + \left(z - \frac{l}{2}\right)^2}}{r_1 + \sqrt{r_1^2 + \left(z - \frac{l}{2}\right)^2}}\right\} \tag{9}$$

where l, r_1, r_2, and N are the kicker length, inner and outer radii, and number of turns, respectively, and I_k is the kicker current. The kicker axial field in our experiment (~2 kG on-axis) is opposite to the solenoid field. The effect of the kicker coil as a means to spin up the electrons is demonstrated in Fig. 7. An electron injected into the coil parallel to its axis acquires a transverse velocity component, and enters into cyclotron motion along the solenoid bore. The parameters are $N = 36$, $I_k = 100$ A, $I_{eb} = 0.2$ A, $V_{eb} = 8$ kV, and $B_{\text{sol}} = 4$ KG. The ratio $\overline{\beta}_{e\perp}/\overline{\beta}_{ez}$ induced by the kicker is of the order of one.

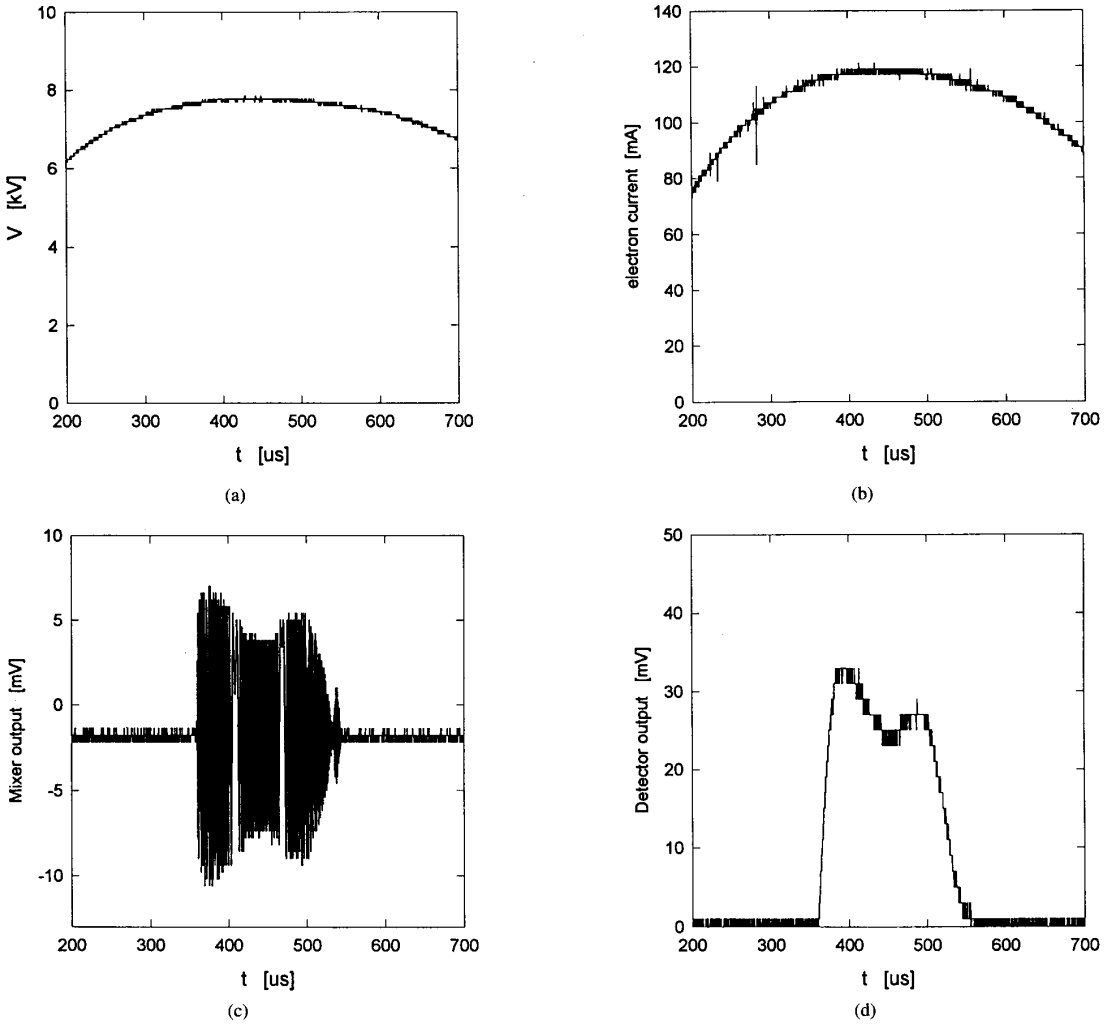

Fig. 10. A typical experimental result of the periodic-waveguide cyclotron oscillator. (a) An electron gun voltage trace. (b) The e-beam current measured in the collector. (c) The heterodyne mixer output. (d) A microwave detected power trace.

It should be noted that in [1] and [2], unlike the oscillator experiment presented here, amplification is observed without any imposed kicker field at the entrance. Reference [19] provides a theoretical explanation for amplification without initial transverse velocity when the $e2$ term in (4) is dominant.

C. Electrical Circuits

The electrical circuitry in the cyclotron experiment incorporates three high voltage pulsers, for the e gun, the solenoid, and the kicker, as shown in the block diagram in Fig. 3. The detailed electronic design of these pulsers is described in [27].

The solenoid pulser generates a 650-V, 30-ms pulse that corresponds to a peak magnetic field of 4 kG. The kicker and the electron gun pulsers are triggered near the peak of the solenoid pulse as shown in the timing diagram in Fig. 4. The e-gun pulse reaches 10 kV and its pulse width is 1 ms. The kicker coil can produce 7 kG maximum magnetic field on axis.

The high-voltage electron gun pulser, based on a standard car ignition transformer coil, is shown schematically in Fig. 8. A 300-μF capacitor bank is charged initially to 600 V by a charging circuit. The capacitor is discharged into the primary winding of the ignition coil by an SCR (CS35-08i04) triggered by a control circuit at the peak of the solenoid pulse. The 1N5408 diode prevents a damaging recharge of the electrolytic capacitor. The secondary winding produces the high-voltage pulse and is connected directly to the electron gun with no need for any high-voltage switching. This circuit design was proved to be a reliable low-cost solution for a table-top experiment.

D. RF Diagnostics

The RF power that is generated in the cyclotron oscillator is detected by the apparatus shown in Fig. 9. The output signal is sampled by a 20-dB cross coupler inside the cavity. The signal is attenuated by a 30-dB attenuator in each output terminal of the coupler. In one arm, the attenuated signal is detected by an

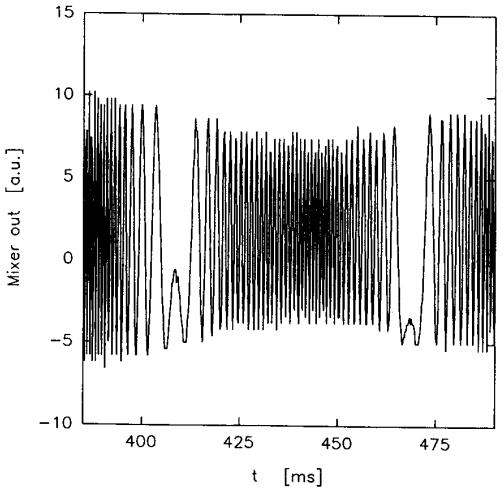

(a)

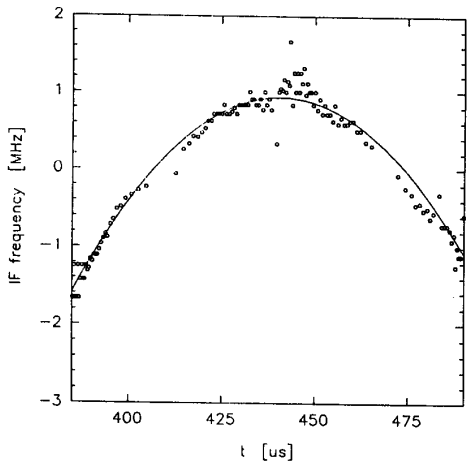

(b)

Fig. 11. Chirping effect due to the electron energy variation. (a) An expansion of the IF signal in Fig. 10(c). (b) The intermediate frequency. The dots represent 1/period of each period. The solid line is their second order curve fit.

HP424A power detector. In the other arm, the attenuated signal is mixed with a 9.4-GHz fixed-frequency signal generated by an external RF oscillator. The mixer output is filtered by the internal 20 MHz low-pass filter of a Tektronix TDS 540 digital oscilloscope. The mixer output shows the laser frequency shifted by 9.4 GHz. Typical signal measurements are presented in the next section.

IV. Experimental Results

Fig. 10(a)–(d) show a typical measurement in the periodic-waveguide cyclotron oscillator experiment. Fig. 10(a) shows the e-gun voltage variation during the pulse. Fig. 10(b) shows the corresponding e-beam current measured in the collector section. Fig. 10(c) and (d) show the microwave heterodyne detection output and the corresponding microwave power detection output, respectively.

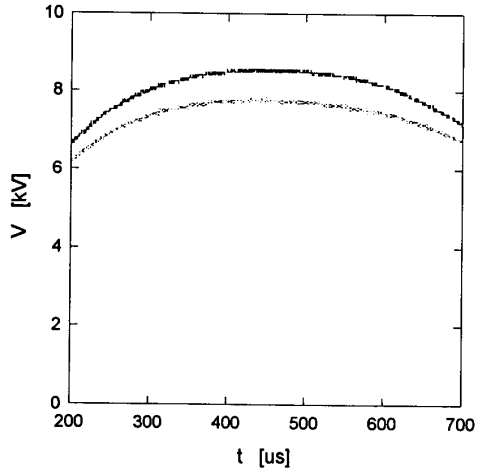

(a)

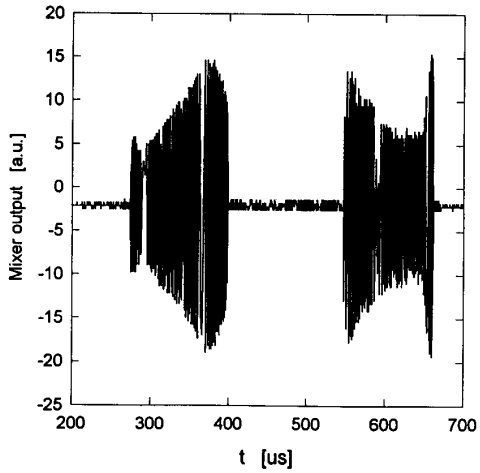

(b)

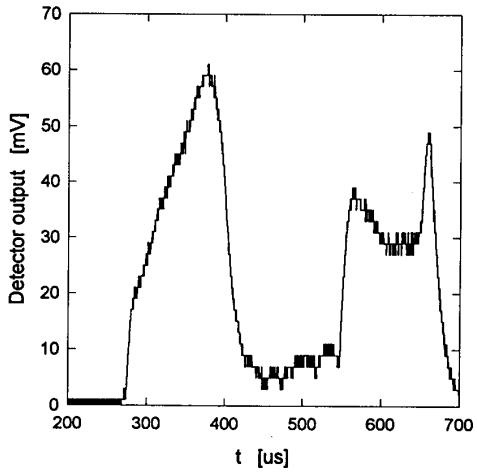

(c)

Fig. 12. An example of the periodic-waveguide cyclotron operation with a slightly too-high electron beam energy. (a) The electron gun voltage trace (the dotted line shows the voltage trace of Fig. 10(a) for comparison). (b) The heterodyne mixer output (note the two separate pulses in comparison with the single pulse in Fig. 10(c)). (c) The microwave detected power trace.

A frequency sweep (i.e., chirping) is observed in the mixing output in Fig. 10(c). According to the tuning relation of (1), this sweep results from the electron energy variation shown in Fig. 10(a). The two nulls in the heterodyne output signal in Fig. 10(c) represent the crossing of the maser frequency sweep through the local oscillator frequency of 9.40 GHz. Using (1), we can obtain the wavenumber at which the interaction occurs by $\beta \cong (\omega - \omega_c)/V_{0z}$. The maser output frequency at the nulls is $\omega \cong \omega_{LO} = 2\pi$ (9.40) GHz. The cyclotron frequency is computed from the axial magnetic field measurement (Fig. 4), and gives $\omega_c \sim 2\pi$ (11.0) GHz. The electron axial velocity is determined from the voltage measurement in Fig. 10(a) and (8a)–(8b), and gives $V_{0z} \sim 0.12$ c. This gives $\beta \sim -280$ m^{-1}, and a corresponding guide wavelength of 2.2 cm. The negative sign indicates that the periodic waveguide cyclotron oscillator interacts with a backward-propagating wave. However, unlike a conventional BWO operation, here the group velocity is positive and the phase velocity is negative. This result differs also from the MIT cyclotron amplifier experiment [1], [2] in which the interaction occurred with a forward wave near cutoff.

The instantaneous intermediate frequency of the IF signal shown in Fig. 11(a) (an expansion of Fig. 10(c)) is presented in Fig. 11(b) as obtained from 1/period of each period in the IF signal. The solid line in Fig. 11(b) is a second order curve fit of the IF frequency variation. It follows accurately the curvature of the electron energy sweep shown in Fig. 10(a), in accordance with expectations.

The effect of a slight detuning of the peak electron beam energy is demonstrated in Fig. 12(a)–(c). The peak e-beam in this shot (8.5 keV) is higher than the optimal peak energy in Fig. 10(a) (7.8 keV) whereas the axial magnetic field is the same in both runs (4 kG). Hence, the cyclotron oscillator emits two separate microwave pulses as shown in the mixer output in Fig. 12(b), and in the corresponding detector output in Fig. 12(c). The interaction occurs below the peak energy, namely at the leading and the trailing edges of the e-beam pulse. That is, the e-beam energy between the two signals of Fig. 12(b) and 12(c) is too high to fulfill the cyclotron resonance condition.

The effective output power and the corresponding efficiency of the periodic-waveguide cyclotron-resonance maser are measured by an external loading of the oscillator cavity, as shown in Fig. 13(a). The dissipated RF power is sampled by a detector through a 20 dB coupler and a 36 dB attenuator. Fig. 13(b) shows output microwave pulses of ~0.4 kW peak power with the corresponding electron-gun voltage. Microwave outputs of >0.3 kW have been observed routinely in similar conditions. These measurements lead to an efficiency estimate of >20% for this oscillator.

The cyclotron-resonance maser oscillator experiment has been operated successfully for several months with hundreds of shots and has been proven as a reliable experimental device.

V. Conclusion

The periodic-waveguide cyclotron oscillator experiment shows strong cyclotron interaction between a low-energy

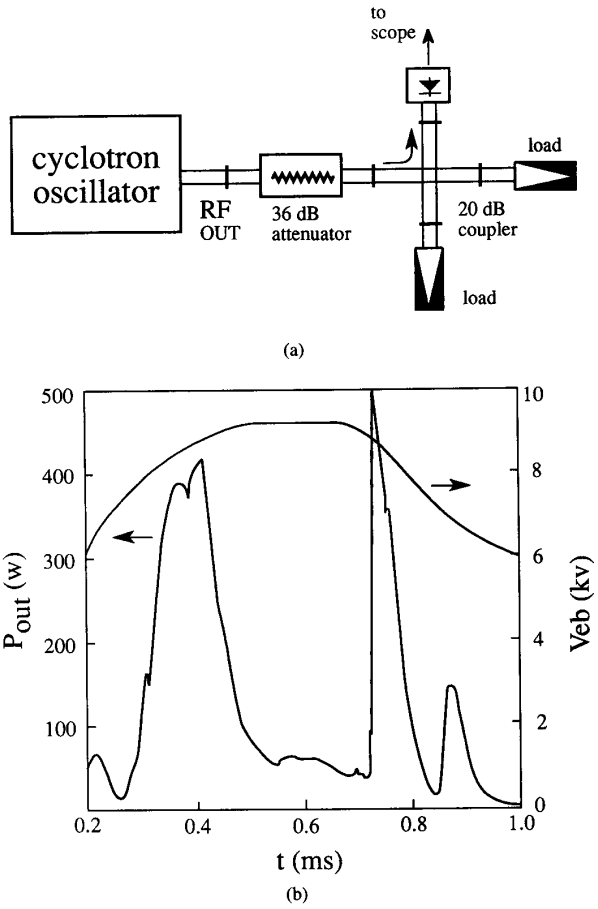

Fig. 13. Microwave output power measurement. (a) The external dummy load and the dissipated power sampling. (b) The oscillator output power and the corresponding electron gun voltage.

electron beam in an axial magnetic field and a traveling wave in a periodic waveguide. The coupling occurs at a wave frequency which is slightly lower than the electron cyclotron frequency, hence, with a backward harmonic of the periodic waveguide. The relatively high efficiency measured in this experiment (>20%), without any efficiency enhancement mechanism, coincides with the large electron-energy acceptance observed in our previous periodic-waveguide cyclotron maser experiments [1]–[4].

A linear model of the periodic-waveguide cyclotron interaction [19] predicts that amplification can also occur due to the inductive impedance of the periodic waveguide near cutoff, even in the absence of an initial electron transverse velocity. In the present experiment, however, oscillations are observed only with a relatively strong magnetic kicker that induces initial transverse velocity at the entrance to the interaction region.

A further study is needed to investigate the effects of the waveguide impedance, dispersion, and losses, and initial electron transverse velocity. Our recent amplifier and oscillator experiments show, however, the feasibility of a compact periodic-waveguide cyclotron maser device using nonrelativis-

tic electron beams ($\sim$ 10 kV), unlike conventional cyclotron masers and gyrotrons, which require beam energies of $\sim$ 100 kV and higher.

ACKNOWLEDGMENT

The authors wish to thank the technical staff of the Tel Aviv University Faculty of Engineering; Mrs. L. Sabag, D. Armoni, S. Moshel, S. Balavis, and E. Nevo for their contribution to the design and construction of the experimental setup, and Mr. Eckardt Whu for the developing of the data acquisition software for this experiment.

REFERENCES

[1] E. Jerby and G. Bekefi, "Nonrelativistic traveling wave cyclotron interaction," *Proc. SPIE*, vol. 1872, pp. 276–293, 1993.
[2] ——, "Cyclotron maser experiments in a periodic waveguide," *Phys. Rev. E*, vol. 48, pp. 4637–4641, 1993.
[3] E. Jerby, G. Bekefi, and A. Shahadi, "Observation of frequency modulation effect in a periodic waveguide cyclotron free-electron maser," presented at the *15th FEL Conf. Proc.*, The Hauge, The Netherlands, 1993; also in *Nuclear Instrum. and Methods*, vol. A341, pp. 115–118, 1994.
[4] E. Jerby, G. Bekefi, A. Shahadi, E. Agmon, H. Golombek, V. Grinberg, and M. Bensal, "Backward wave cyclotron maser oscillator experiment," *SPIE Conf. on Intense Microwave Pulses*, Los Angeles, CA, Jan. 22–29, 1994.
[5] K. R. Chu, P. Sprangle, and V. L. Granatstein, "Theory of a dielectric loaded cyclotron travelling wave amplifier," *Bull. Amer. Phys. Soc.*, vol. 23, p. 748, 1978.
[6] J. M. Baird, S. Y. Park, K. R. Chu, H. Keren, and J. L. Hirshfield, "Design of a slow-wave cycltron amplifier," *Bull. Amer. Phys. Soc.*, vol. 25, p. 911, 1980.
[7] K. R. Chu, A. K. Ganguly, V. L. Granatstein, J. L. Hirshfield, S. Y. Park, and J. M. Baird, "Theory of a slow wave cyclotron amplifier," *Int. J. Electron.*, vol. 51, pp. 493–502, 1981.
[8] H. Guo, L. Chen, H. Keren, and J. L. Hirshfield, "Measurements of gain for slow cyclotron wave on an annular electron beam," *Phys. Rev. Lett.*, vol. 49, pp. 730–733, 1982.
[9] D. B. McDermott, H. B. Cao, and N. C. Luhmann, "Cherenkov cyclotron autoresonance maser," *Int. J. Electron.*, vol. 65, p. 477, 1988.
[10] T. H. Kho and A. T. Lin, "Slow wave electron cyclotron maser," *Phys. Rev. A*, vol. 38, pp. 2883–2888, 1988.
[11] H. B. Cao, D. B. McDermott, and N. C. Luhmann, "Initial operation of a Cherenkov CARM," *Proc. SPIE*, vol. 1061, pp. 248–253, 1989.
[12] A. K. Ganguly and S. Ahn, "Nonlinear theory for the slow wave cyclotron interaction," *Phys. Rev. A*, vol. 42, pp. 3544–3554, 1990.
[13] K. C. Leou, D. B. McDermott, and N. C. Luhmann Jr., "Dielectric-loaded wideband gyro-TWT," *IEEE Trans. Plasma Sci.*, vol. 20, pp. 188–196, 1992.
[14] J. L. Hirshfield and J. M. Wachtel, "Electron Cyclotron Maser," *Phys. Rev. Lett.*, vol. 12, pp. 533–536, 1964.
[15] J. L. Hirshfield and V. L. Granatstein, "The electron cyclotron maser—an historical survey," *IEEE Trans. Microwave Theory Tech.*, vol. 25, pp. 522–527, 1977.
[16] J. M. Baird, "Gyrotron theory," *High Power Microwaves*, V. L. Granatstein and I. Alexeff, Eds. Artech House, 1987.
[17] V. L. Bratman, N. S. Ginzburg, G. S. Nusinovich, M. I. Petelin, and P. S. Strelkov, "Relativistic gyrotrons and cyclotron autoresonance masers," *Int. J. Electron.*, vol. 51, pp. 541–567, 1981.
[18] A. C. DiRienzo, G. Bekefi, C. Chen, and J. S. Wurtele, "Experimental and theoretical studies of a 35 GHz cyclotron autoresonance maser amplifier," *Phys. Fluids*, vol B3, pp. 1755–1765, 1991.
[19] E. Jerby, "Linear analysis of periodic waveguide cyclotron maser," *Phys. Rev. E*, vol. 49, pp. 4487–4496, 1994.
[20] E. Agmon, H. Golombek, and E. Jerby, "Traveling-wave free-electron maser experiment," *Nuclear Instrum. and Methods*, vol. A331, pp. 156–159, 1993.
[21] R. E. Collin, *Field Theory of Guided Waves*. New York: McGraw-Hill, 1960.
[22] A. M. Model, N. S. Belevitch, "Calculation of the loaded Q-factor of waveguide resonators formed by grid diaphragms," *Telecomm. Radio Eng. (USA)*, vol. 18, pp. 15–26, 1963.
[23] H. Guo, Y. Carmel, W. R. Lou, L. Chen, J. Rodgers, D. K. Abe, A. Bromaborsky, W. Destler, and V. L. Granatstein, "A novel highly accurate synthetic technique for determination of the dispersive characteristics in periodic slow wave circuits," *IEEE Trans. Microwave Theory Tech.*, vol. 40, pp. 2086–2094, 1992.
[24] Y. Leviatan, P. G. Li, A. T. Adams, and J. Perini, "Single post inductive obstacle in rectangular waveguide," *IEEE Trans. Microwave Theory Tech.*, vol. 31, pp. 806–811, 1983.
[25] E. Agmon, M.Sc. thesis, Tel Aviv University, in preparation.
[26] G. A. Nagy and M. Szilgyi, *Introduction to the Theory of Space-Charge Optics*. New York: Halsted Press, John Wiley, 1974.
[27] V. Grinberg, E. Jerby, and A. Shahadi, "Low-cost electron gun pulser for table-top maser experiments," *Nuclear Instrum. and Methods*, in press.

Eli Jerby was born in Israel in 1957. He received the B.Sc. and M.Sc. degrees in 1980, and his Ph.D. degree in 1989, all from Tel-Aviv University.

In 1989, he joined MIT as a postdoctoral Fulbright and Rothschild fellow under the supervision of Professor George Bekefi. In 1991, he was appointed as a lecturer at Tel-Aviv University, where he established an experimental research group studying high-power microwave generation by new schemes of low-voltage cyclotron-resonance and free-electron masers.

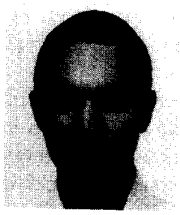

Avi Shahadi received the B.Sc. degree in electrical engineering at Tel-Aviv University in 1993.

He joined the high power microwave laboratory at TAU in 1992. Currently, he is completing his M.Sc. degree on compact, low-voltage gyrotron devices.

Vladimir Grinberg was born in Blagoveshchensk-on-Amur, Russia, in 1946. He received the high school diploma (in 1968) and the Cand.Sc. degree (in 1974) from the Polytechnic Institute of Tomsk, Russia.

Since June 1992, he has been with the high-power microwave laboratory at the Faculty of Engineering of the University of Tel-Aviv, Israel. He is the author of 15 inventions and over 25 technical journal papers on transient processes theory and electromagnet systems with magnetic-field forcing, alternating-current electrical machines, and electromotors with built-in brakes.

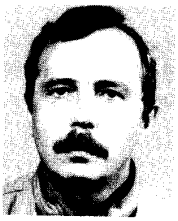

Vladimir Dikhtiar received the M.S. degree in radiophysics from the National University of Sarato, Russia, in 1970, and the Ph.D. degree in electrical engineering from the Moscow Institute of Radio Engineering and Electronics of the USSR Academy of Sciences in 1975.

From 1975, he was with the Moscow Institute of Radio-Engineering and Electronics as a Research Associate. He emigrated to Israel in 1991. Currently, he is a Research Associate at Tel-Aviv University. His research interests include scattering analysis of active and passive microwave devices.

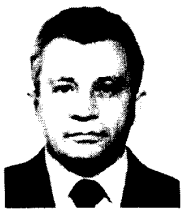

Marat Sheinin was born in Minsk, USSR in 1932. He received the M.Sc. degree in radio technology from the Institute of Minsk, USSR in 1962.

Since then he has worked as a microwave engineer in Russia. He is the author of six patents. He emigrated to Israel in 1990 and continued to work on various projects of Gunn diode generators. Since 1992, he has been working at the University of Tel-Aviv, Israel. His research interests include theoretical and practical issues on microwave oscillators.

Eran Agmon was born in Israel in 1964. He received his B.Sc. degree in electrical engineering from the Tel Aviv University in 1991, and joined the cyclotron research group as a graduate student.

From 1992 to 1994, he worked for Elisra Electronic Systems Ltd. in developing high-power solid-state amplifiers. Since 1994, he is with the R&D group of Gilat Satelite Netwotks Ltd.

Harel Golombek was born in Tel Aviv, Israel, in 1964. He received his B.Sc. degree in electrical engineering from the Tel Aviv University in 1986.

Since 1987, he is employed as an antenna engineer by the I.D.F. In 1991–1992, he worked with the cyclotron research group as a graduate student.

Vitaly Trebich received the M.Sc. degree in electronic engineering from the Leningrad North-Western Polytechnic Institute in 1970, and the Ph.D. degree from the Radiotechnical Institute of the former USSR Academy of Science, Moscow, in 1986.

He worked in the UHF Electronics and Electrodynamic Laboratory at the Institute of Electrical Engineering, Leningrad, until 1991. From 1991 to 1993, he was a research fellow at the Tel Aviv University. His research interests include theoretical and practical issues in microwave engineering.

Dr. Trebich is the author of six patents and more than 21 journal papers.

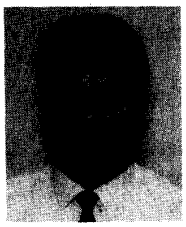

Moshe Bensal (M'79–M'93) was born in Istanbul, Turkey, in 1948. He emigrated to Israel in 1949. In 1978, he joined Elisra Ltd. as a microwave technician. Since 1987, he is working as a research technician at Tel Aviv University.

G. Bekefi, photograph and biography not available at the time of publication.